Ab Initio Elasticity of Poly(lactic acid) Crystals

Tingting Lin,[†,‡] Xiang-Yang Liu,[‡] and Chaobin He*[,†]

Institute of Materials Research and Engineering, ASTAR (Agency for Science, Technology and Research), 3 Research Link, Singapore 117602, and Department of Physics, National University of Singapore, 2 Science Drive 3, Singapore 117542

Received: November 25, 2009; Revised Manuscript Received: January 19, 2010

We investigate the elastic properties of poly(lactic acid) crystals using a first-principles pseudopotential plane wave method within the generalized gradient approximation of the density functional theory. Stiffness and compliance matrices of poly(L-lactic acid) (PLLA) α- and β-forms, and the stereocomplex (sc) between PLLA and poly(D-lactic acid) (PDLA) (50:50) sc-form are calculated using the finite strain technique. The results indicate that crystalline poly(lactic acid) is highly mechanical anisotropic. Contributions from the crystalline phase to the anisotropy of the elastic modulus in an uniaxially oriented poly(lactic acid) fiber are estimated on the basis of a cylindrically symmetric polycrystalline aggregate model. Both symmetry and orientation distribution of the crystals have been taken into account. Voigt and Reuss bounds of Young's moduli and shear moduli and Poisson's ratio are calculated from single crystal elastic properties.

1. Introduction

Poly(lactic acid) (PLA) is a biodegradable and biocompatible semicrystalline polymer with high tensile strength and Young's modulus[1,2] and high shear piezoelectric constant.[3,4] Fibers made of PLA or its copolymers are widely used as sutures. PLA screws and pins are used as orthopedic implants. Currently, studies have been carried out to investigate the potential of using piezoelectric PLLA fiber as a tweezer to manipulate cells.[5] Therefore, knowledge of stiffness and compliance of PLA is essential for many practical applications related to the mechanical and piezoelectric properties. However, no measurement of instinct elastic constants of PLA single crystal has been performed due to the polymer semicrystalline character and the difficulty of preparing a 100% crystalline sample. Computer calculations on the molecular level could be a complement to the lack of experimental data.

The low energy conformation of an isolated PLA chain is a helix, either 10_3 or 3_1. PLA can crystallize in different phases: poly(L-lactic acid) (PLLA) α-, β-, and γ-forms, and the stereocomplex (sc) between PLLA and poly(D-lactic acid) (PDLA) (50:50) sc-form.[6−9] Various unit cells have been proposed from X-ray scattering data combining with empirical molecular simulations.[9−13] We have employed the density functional theory (DFT) method to further optimize the geometries of these unit cells. By comparing monomer energy in the optimized unit cells, we found that the stability order is sc-form > α-form > β-form > γ-form and for the three different PLLA α-form unit cells, α-form-2003 (Sasaki and Asakura)[12] > α-form-2001 (Aleman et al)[11] > α-form-1995 (Kobayashi et al).[10] That is, we have proved theoretically that the sc-form is the most energetically favored among the various polymorphs and the two helical PLLA chains in the α unit cell when packing in antiparallel is more stable than in parallel on the basis of the ab initio calculations.

The determination of the stiffness and compliance constants in the crystalline regions of polymers is important for giving bounds against which practice can achieve. De Oca and Ward[14] calculated the stiffness and compliance matrices of PLLA α-phase[10] by minimizing a strained (0.15%) unit cell potential energy employing a force field. A chain modulus of 35 GPa and a shear (parallel to the helical axis) modulus of 3 GPa were predicted. They attributed the low shear modulus to the effect of bond rotation (because of the PLLA molecular helical conformation) on the deformation. However, they also found considerable changes in the unit cell lattice constants and angles (i.e., from $a = 1.05$ nm, $b = 0.61$ nm, $c = 2.88$ nm, $\alpha = \beta = \gamma = 90°$ to $a = 1.09$ nm, $b = 0.52$ nm, $c = 3.39$ nm, $\alpha = 94°$, $\beta = 91°$, $\gamma = 64°$) during geometry optimization and suspected this may be caused by the inadequate estimation of the intermolecular interactions with the forcefield used. Actually the crystal structure has already changed significantly and may not be in the elastic strain range. Among the stiffness coefficients, only the value of c_{33} was reported with confidence. The existing uncertainty with regards to the accuracy on other stiffness coefficients of α-PLLA provides a motivation for the present study. In addition, there has been no theoretical elastic data reported yet for PLA other polymorphs.

Empirical models are known to produce errors on the order of at least 10−15% for the diagonal components of the stiffness tensor, and the off-diagonal components are predicted even less reliably. It is thus preferable to base the calculation of elastic stiffness and compliance coefficients on a quantum-mechanical description. The first principle calculations have shown reliable results in prediction of elastic properties of inorganic compounds for a large variety of materials: metals, semiconductors, insulators and alloys etc.[15−18] In this paper, we report the results of a systematic ab initio study of the elastic properties of various crystalline PLA phases. We have used ab initio method by means of the CASTEP (**Ca**mbridge **S**erial **T**otal **E**nergy **P**ackege) software,[19] employing the generalized gradient approximation (GGA) within density functional theory (DFT).[20,21]

2. Computational Details

According to the generalized Hooke's law, the stress (σ_{ij}) and strain (ε_{ij}) for small deformations to a crystal are linearly

* Corresponding author. E-mail: cb-he@imre.a-star.edu.sg.
† ASTAR.
‡ National University of Singapore.

10.1021/jp911198p
Published on Web 02/12/2010

TABLE 1: Three Initial PLA Crystalline Unit Cells Built for This Study

crystal code	symmetry group, crystal system, crystal class	lattice constants (Å); angles (deg); volume (Å^3); density (g/cm^3); no. of atoms	ref	no. of independent; stiffness c_{ij} (in the Voigt notation)
α-form	*P*212121, orthorhombic, 222	$a = 10.661$, $b = 6.161$, $c = 28.882$; $\alpha = \beta = \gamma = 90$; $V = 1897.04$; $d = 1.262$; 180 ($C_{60}H_{80}O_{40}$)	12	9; c_{11}, c_{22}, c_{33}, c_{44}, c_{55}, c_{66}, c_{12}, c_{13}, c_{23}
β-form	*P*32, trigonal, 3	$a = b = 10.52$, $c = 8.8$; $\alpha = \beta = 90$, $\gamma = 120$; $V = 843.42$; $d = 1.277$; 81 ($C_{27}H_{36}O_{18}$)	13	7; c_{11}, c_{33}, c_{44}, c_{12}, c_{13}, c_{14}, c_{15}, $c_{22} = c_{11}$, $c_{55} = c_{44}$, $c_{23} = c_{13}$, $-c_{24} = c_{56} = c_{14}$, $c_{25} = c_{46} = -c_{15}$, $c_{66} = (c_{11} - c_{12})/2$
sc-form	*R*3*c*, trigonal, 3*m*	$a = b = 14.98$, $c = 8.8$; $\alpha = \beta = 90$, $\gamma = 120$; $V = 1710.160$; $d = 1.260$; 162 ($C_{54}H_{72}O_{36}$)	9	6; c_{11}, c_{33}, c_{44}, c_{12}, c_{13}, c_{14}, $c_{22} = c_{11}$, $c_{55} = c_{44}$, $c_{23} = c_{13}$, $-c_{24} = c_{56} = c_{14}$, $c_{66} = (c_{11} - c_{12})/2$

related by $\sigma_{ij} = c_{ijkl}\varepsilon_{kl}$ ($i, j, k, l = 1, 2, 3$) or inversely $\varepsilon_{ij} = s_{ijkl}\sigma_{kl}$ ($i, j, k, l = 1, 2, 3$), where c_{ijkl} is called the stiffness and s_{ijkl} the compliance tensor. In the matrix representation, according to the Voigt notation, the stress−strain relation becomes $\sigma_p = c_{pq}\varepsilon_q$ or $\varepsilon_p = s_{pq}\sigma_q$, where $p, q = 1, 2, ..., 6$.

There are two major approaches, stress−strain[22] and energy−strain,[23] available for computation of stiffness coefficients of a solid. Practical methods for determining the stiffness coefficients from first principles usually set either the stress or strain to a finite value, optimize any free parameters of the structure, and calculate the other property−strain or stress, respectively. Applying a given homogeneous deformation (the strain) and calculating the resulting stress requires less computational effort, since the unit cell is fixed and only the ionic positions require optimization. This is the method implemented in the present work. In this finite strain approach, the ground-state structure is strained according to symmetry-dependent strain patterns with varying amplitudes. The full elastic tensors are determined from the computation of the stresses generated by the small deformations after a reoptimization of the internal structure parameters, i.e., after a geometry optimization with fixed strained cell parameters.

The elastic stiffness tensors were calculated for the structures corresponding to the theoretical ground states (geometry optimization). The starting point for the geometry optimization is the experimentally determined structures. Table 1 summarizes the details of the three unit cells in this study. During the ground states' geometry optimization, we did not optimize the lattice parameters because the calculated densities of the starting structures (in grams per cm^3), 1.262 (α-form), 1.277 (*β*-form), and 1.260 (sc-form), as shown in Table 1, are already in the range of experimental measurements (1.290 g/cm^3 for crystalline phase, 1.248 g/cm^3 for completely amorphous phase).[24] In addition, it is known that DFT GGA approximation would overestimate the volumes of crystals.[25,26] Therefore, during the optimization, lattice constants of the unstrained unit cells were fixed to those values determined in XRD experiments. Only the positions of atoms in the unit cell were fully relaxed. The high symmetries presented in PLA crystals cut the number of independent stiffness constants to less than 10, as indicated in Table 1, which helps to reduce the computation expense greatly.

The strained lattice (lattice vectors $\mathbf{a}'$) used to determine the elastic stiffness is related to the unstrained lattice ($\mathbf{a}$) by $\mathbf{a}' = (\mathbf{I} + \boldsymbol{\varepsilon})a$, where $\mathbf{I}$ is the identity matrix and $\boldsymbol{\varepsilon}$ the strain tensor. All the strain tensors used in this work are listed in the follows (A1)−(A5).

$$\boldsymbol{\varepsilon} = \begin{pmatrix} \varepsilon & 0 & 0 \\ 0 & 0 & \varepsilon/2 \\ 0 & \varepsilon/2 & 0 \end{pmatrix} \quad \text{(A1)}$$

$$\boldsymbol{\varepsilon} = \begin{pmatrix} 0 & \varepsilon/2 & 0 \\ \varepsilon/2 & 0 & 0 \\ 0 & 0 & \varepsilon \end{pmatrix} \quad \text{(A2)}$$

$$\boldsymbol{\varepsilon} = \begin{pmatrix} 0 & 0 & \varepsilon/2 \\ 0 & \varepsilon & 0 \\ \varepsilon/2 & 0 & 0 \end{pmatrix} \quad \text{(A3)}$$

$$\boldsymbol{\varepsilon} = \begin{pmatrix} \varepsilon & 0 & 0 \\ 0 & 0 & 0 \\ 0 & 0 & 0 \end{pmatrix} \quad \text{(A4)}$$

$$\boldsymbol{\varepsilon} = \begin{pmatrix} 0 & 0 & 0 \\ 0 & 0 & \varepsilon/2 \\ 0 & \varepsilon/2 & \varepsilon \end{pmatrix} \quad \text{(A5)}$$

A set of linear equations, which represents the general Hooke's law for a crystal, are constructed from the calculated stress generated by specific deformations to the crystal. For example, the PLLA α-phase is an orthorhombic crystal, which has nine different symmetry elements (c_{11}, c_{22}, c_{33}, c_{44}, c_{55}, c_{66}, c_{12}, c_{13}, and c_{23}). Three different strain patterns, (A1)−(A3), are needed to give stresses related to all the nine independent c_{pq} (from strain pattern (A1), $\sigma_1^{A1} = c_{11}\varepsilon^{A1}$, $\sigma_2^{A1} = c_{12}\varepsilon^{A1}$, $\sigma_3^{A1} = c_{13}\varepsilon^{A1}$, $\sigma_4^{A1} = c_{44}\varepsilon^{A1}$; from pattern (A2), $\sigma_1^{A2} = c_{13}\varepsilon^{A2}$, $\sigma_2^{A2} = c_{23}\varepsilon^{A2}$, $\sigma_3^{A2} = c_{33}\varepsilon^{A2}$, $\sigma_6^{A2} = c_{66}\varepsilon^{A2}$; and from pattern (A3), $\sigma_1^{A3} = c_{12}\varepsilon^{A3}$, $\sigma_2^{A3} = c_{22}\varepsilon^{A3}$, $\sigma_3^{A3} = c_{23}\varepsilon^{A3}$, $\sigma_5^{A3} = c_{55}\varepsilon^{A3}$) for the orthorhombic system. Similarly, for trigonal systems: PLLA *β*-phase and PLLA:PDLA = 50:50 stereocomplex crystal, the strain tensors (A4) and (A5) were used in both cases (for *β*-phase, from pattern (A4): $\sigma_1^{A4} = c_{11}\varepsilon^{A4}$, $\sigma_2^{A4} = c_{12}\varepsilon^{A4}$, $\sigma_3^{A4} = c_{13}\varepsilon^{A4}$, $\sigma_4^{A4} = c_{14}\varepsilon^{A4}$, $\sigma_5^{A4} = c_{15}\varepsilon^{A4}$; from pattern (A5): $\sigma_1^{A5} = (c_{11} + c_{14})\varepsilon^{A5}$, $\sigma_2^{A5} = (c_{11} - c_{14})\varepsilon^{A5}$, $\sigma_3^{A5} = c_{33}\varepsilon^{A5}$, $\sigma_4^{A5} = c_{44}\varepsilon^{A5}$, $\sigma_6^{A5} = -c_{15}\varepsilon^{A5}$; for sc-form, similar to those of *β*-form, but $c_{15} = 0$). The system of over determined linear equations are solved to obtain a complete set of independent stiffness constants. Two positive and two negative amplitudes were used for each strain with maximum value of 0.3%. The elastic stiffness coefficients were then determined from a linear fit of the calculated stress as a function of strain.

It is computer-time intensive to calculate the stiffness of a polymer crystal with tens to hundreds atoms per unit cell using the ab initio method. In our calculations, some approximations have been made. All the quantum-mechanical calculations were performed on the basis of DFT implemented in CASTEP. Electron−ion interactions were described by ultrasoft psedopotentials,[27] which require significantly less computational resources than norm-conserving potentials, and electronic wave functions were represented using a plane-wave basis set[28] with an energy cutoff of 340 eV. Exchange−correlation effects were taken into account using the form of Perdew and Wang generalized gradient approximation.[29] The Brillouin zone sampling was carried out using a set of Monkhorst−Pack points with a grid spacing smaller than 0.04 Å^{-1}.[30] The major advantage of the plane-wave based approach is the ease of computing forces and stresses. The coordinate optimization is realized using the Broyden−Fletcher−Goldard−Shanno (BFGS) minimization algorithm by taking into account the total energy as well as the gradients to relax the atomic position.

Calculations were considered to be converged when the maximum force on an atom was below 0.02 eV/Å and maximum displacement below 0.001 Å. Energy converged to better than 1.0×10^{-5} eV/atom.

3. Results and Discussion

3.1. Stiffness and Compliance Matrices of the Poly(lactic acid) Single Crystals. The calculated full matrices: stiffness c_{pq} (in GPa) and compliance s_{pq} (in GPa^{-1}) for the three PLA polymorphs are

$$(c_{pq})^{\alpha-form} = \begin{pmatrix} 15.34 & 5.25 & 10.01 & 0 & 0 & 0 \\ 5.25 & 7.67 & 10.26 & 0 & 0 & 0 \\ 10.01 & 10.26 & 28.62 & 0 & 0 & 0 \\ 0 & 0 & 0 & 13.0 & 0 & 0 \\ 0 & 0 & 0 & 0 & 8.16 & 0 \\ 0 & 0 & 0 & 0 & 0 & 3.63 \end{pmatrix}$$

$$(s_{pq})^{\alpha-form} = \begin{pmatrix} 0.0897 & -0.0374 & -0.0180 & 0 & 0 & 0 \\ -0.0374 & 0.2664 & -0.0825 & 0 & 0 & 0 \\ -0.0180 & -0.0825 & 0.0708 & 0 & 0 & 0 \\ 0 & 0 & 0 & 0.0769 & 0 & 0 \\ 0 & 0 & 0 & 0 & 0.1225 & 0 \\ 0 & 0 & 0 & 0 & 0 & 0.2755 \end{pmatrix}$$

$$(c_{pq})^{\beta-form} = \begin{pmatrix} 16.75 & 13.11 & 18.75 & -2.43 & -0.50 & 0 \\ 13.11 & 16.75 & 18.75 & 2.43 & 0.50 & 0 \\ 18.75 & 18.75 & 30.67 & 0 & 0 & 0 \\ -2.43 & 2.43 & 0 & 9.46 & 0 & 0.50 \\ -0.50 & 0.50 & 0 & 0 & 9.46 & -2.43 \\ 0 & 0 & 0 & 0.50 & -2.43 & 1.82 \end{pmatrix}$$

$$(s_{pq})^{\beta-form} = \begin{pmatrix} 0.2855 & -0.1415 & -0.0880 & 0.1096 & 0.0224 & 0 \\ -0.1415 & 0.2855 & -0.0880 & -0.1096 & -0.0224 & 0 \\ -0.0880 & -0.0880 & 0.14013 & 0 & 0 & 0 \\ 0.1096 & -0.1096 & 0 & 0.1644 & 0 & -0.0447 \\ 0.0224 & -0.0224 & 0 & 0 & 0.1644 & 0.2192 \\ 0 & 0 & 0 & -0.0447 & 0.2192 & 0.8540 \end{pmatrix}$$

$$(c_{pq})^{sc-form} = \begin{pmatrix} 16.75 & 6.69 & 10.50 & 0.13 & 0 & 0 \\ 6.69 & 16.75 & 10.50 & -0.13 & 0 & 0 \\ 10.50 & 10.50 & 24.67 & 0 & 0 & 0 \\ 0.13 & -0.13 & 0 & 0.82 & 0 & 0 \\ 0 & 0 & 0 & 0 & 0.82 & 0.13 \\ 0 & 0 & 0 & 0 & 0.13 & 5.03 \end{pmatrix}$$

$$(s_{pq})^{sc-form} = \begin{pmatrix} 0.0844 & -0.0154 & -0.0293 & -0.0156 & 0 & 0 \\ -0.0154 & 0.0844 & -0.0293 & 0.0156 & 0 & 0 \\ -0.0293 & -0.0293 & 0.0655 & 0 & 0 & 0 \\ -0.0156 & 0.0156 & 0 & 1.2210 & 0 & 0 \\ 0 & 0 & 0 & 0 & 1.2210 & -0.0312 \\ 0 & 0 & 0 & 0 & -0.0312 & 0.1996 \end{pmatrix}$$

For all the three crystalline phases, the c_{33} elastic modulus related to the c lattice direction (the helix axis direction, the longitudinal direction) is greater than c_{11} (or c_{22}) related to the lattice a (or b) direction (the lateral, transverse direction). The pure shear elastic modulus c_{66} for the sc-form is larger than $c_{44} = c_{55}$ while opposite trends are found in α- and β-forms. We are not aware of any experimental data on the elastic properties of PLA single crystals. Future experimental measurements will test our calculated predictions.

3.2. Anisotropy of Young's Modulus and Linear Compressibility of the Single Crystals. Nye gave the general expressions of the variations of Young's modulus and linear compressibility with direction for various crystal systems.[31] Here we analyzed some sections of typical surfaces of Young's modulus and linear compressibility for the PLA crystals studied.

3.2.1. Orthorhombic System: PLLA α-Form. The expressions for Young's modulus E and linear compressibility β of the orthorhombic system are in the ab plane:

$$1/E(\varphi) = \cos^4\varphi s_{11} + \sin^4\varphi s_{22} + \cos^2\varphi \sin^2\varphi(2s_{12} + s_{66}) \quad (1)$$

$$\beta(\varphi) = (s_{11} + s_{12} + s_{13})\cos^2\varphi + (s_{12} + s_{22} + s_{23})\sin^2\varphi \quad (2)$$

in the ca plane:

$$1/E(\theta) = \sin^4\theta s_{11} + \cos^4\theta s_{33} + (2s_{13} + s_{55})\sin^2\theta\cos^2\theta \quad (3)$$

$$\beta(\theta) = (s_{11} + s_{12} + s_{13})\sin^2\theta + (s_{13} + s_{23} + s_{33})\cos^2\theta \quad (4)$$

and in the cb plane:

$$1/E(\theta) = \sin^4\theta s_{22} + \cos^4\theta s_{33} + (2s_{23} + s_{44})\sin^2\theta\cos^2\theta \quad (5)$$

$$\beta(\theta) = (s_{12} + s_{22} + s_{23})\sin^2\theta + (s_{13} + s_{23} + s_{33})\cos^2\theta \quad (6)$$

where angle φ is from the a axis and θ from the c axis. Parts a and b of Figure 1 show the anisotropy of Young's modulus ($E(\varphi)$, in GPa) and linear compressibility ($\beta(\varphi)$, in 1/GPa), respectively, and Figure 1c shows the PLLA α-form unit cell projection on the ab plane, The dark blue curves represent the ab initio results (this study) and the pink curves those of the molecular mechanics method.[14] Both studies reveal that for α PLLA Young's modulus in the b direction is smaller than that in the a direction. In other words, it is easier to compress or pull in the b direction than in the a direction. The ab initio curves are more anisotropic.

Similarly, anisotropies in the ca and cb planes are illustrated, respectively, in Figures 2 and 3. The elastic anisotropies on these planes are significantly different between the two sets of curves. The maximum modulus is in the direction deviating from the c axis for the ab initio results (dark blue curves, this work) while being along the c axis for the force field results (the pink curves, De Oca and Ward's[14]). The discrepancy between ours and De Oca and Ward's studies may be due to the different unit cell adopted. The two PLA 10_3 helices pack in parallel in the unit cell proposed by Kobayashi et al. but in antiparallel in that proposed by Sasaki and Asakura. De Oca and Ward[14] used

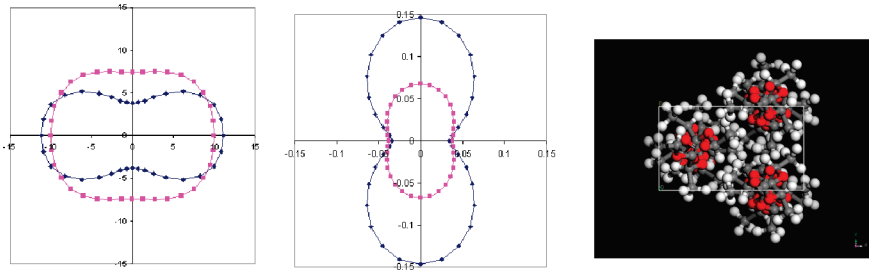

(a) (b) (c)

Figure 1. Comparisons of the variations of (a) Young's modulus and (b) linear compressibility of the PLLA α-form in the *ab* plane (perpendicular to the helix chain axis). (c) Unit cell projection on the *ab* plane. The dark blue curves are plotted using compliance coefficients calculated in this work and the pink curves those from ref 14. The *a* axis is horizontal.

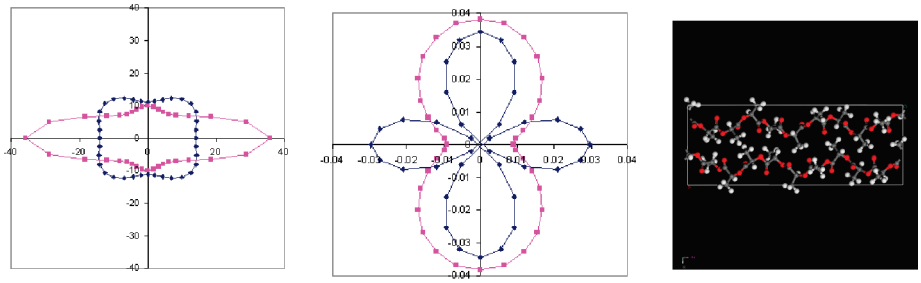

(a) (b) (c)

Figure 2. Comparisons of the variations of (a) modulus and (b) linear compressibility of the PLLA α-form in the *ca* plane (parallel to the helix chain). (c) Unit cell projection on the *ca* plane. The dark blue curves are plotted using compliance coefficients calculated in this work and the pink curves from data in ref 14. The *c* axis is horizontal.

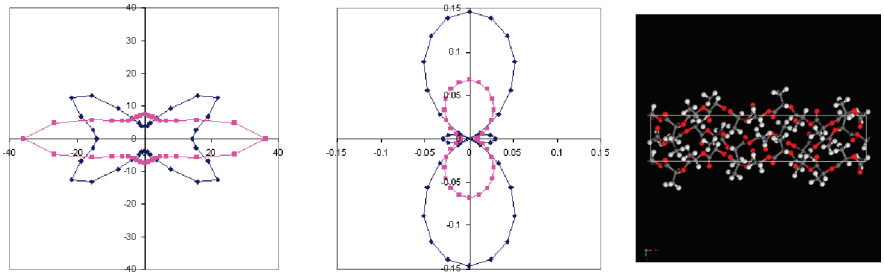

(a) (b) (c)

Figure 3. Comparisons of the variations of (a) modulus and (b) linear compressibility of the PLLA α-form in the *cb* plane (parallel to the helix chain). (c) Unit cell projection on the *cb* plane. The dark blue curves are plotted using compliance coefficients calculated in this work and the pink curves from data in ref 14. The *c* axis is horizontal.

the former. We, however, used the latter because our DFT optimization has shown that it is energetically more favored, as mentioned in the Introduction.

3.2.2. Trigonal System: PLLA β-Form (Class 3), Stereocomplex sc-Form (Class 3m). In the planes perpendicular to the *c* axis (the helix 3_1 axis), for trigonal system (all classes)

$$1/E(\varphi) = s_{11} \tag{7}$$

$$\beta(\varphi) = s_{11} + s_{12} + s_{13} \tag{8}$$

As shown in Figure 4, both the β-form and sc-form are transversely isotropic (in the *ab* plane). The sc-form has a higher Young's modulus and less compressibility than the β-form does.

In a plane perpendicular to the *ab* plane and containing the *c* axis:

$$1/E(\theta,\varphi_0) = \sin^4\theta s_{11} + \cos^4\theta s_{33} + \cos^2\theta \sin^2\theta(2s_{13} + s_{44}) + 2\sin^3\theta\cos\theta\sin\varphi_0(3\cos^2\varphi_0 - \sin^2\varphi_0)s_{14} + 2\sin^3\theta\cos\theta\cos\varphi_0(3\sin^2\varphi_0 - \cos^2\varphi_0)s_{25} \tag{9}$$

$$\beta(\theta,\phi_0) = (s_{11} + s_{12} + s_{13}) - (s_{11} + s_{12} - s_{13} - s_{33})\cos^2\theta \tag{10}$$

where φ_0 is the angle between the plane and *ca* plane. θ is the angle from the *c* axis. For the sc-form the last term in (9) vanishes because $s_{25} = 0$.

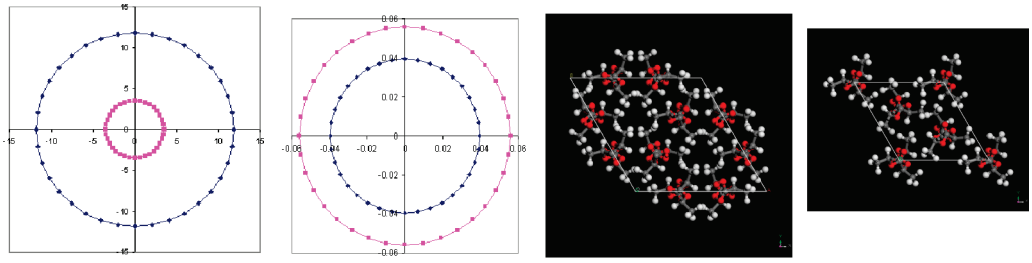

(a) (b) (c) (d)

Figure 4. Comparisons of the variations of (a) modulus and (b) linear compressibility of the PLLA β-form (pink curves) and the stereocomplex between PLLA and PDLA sc-form (dark blue curves) in the *ab* plane (perpendicular to the helix axis). Projections on the *ab* plane of (c) sc-form unit cell and (d) β-form unit cell. The *a* axis is horizontal and the *b* axis is 120° from the *a* axis.

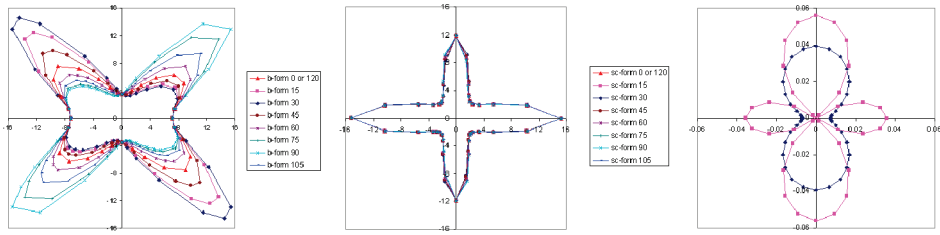

Figure 5. Variations of (a) the modulus of the PLLA β-form and (b) the modulus of the stereocomplex between PLLA and PDLA sc-form (the numbers in the legends indicate constant angle φ_0 (from the *a* axis) values (in degrees). (c) Linear compressibility of β-form (pink curve) and the sc-form (dark blue curve) in a plane perpendicular to the *ab* plane and containing the *c* axis (helix axis). The *c* axis is horizontal.

In Figure 5, on the longitudinal planes, both the β-form and sc-form show anisotropic mechanic behavior. The shape of modulus anisotropy curve of the β-form is very sensitive to the values of φ_0 while that of the sc-form is not. The largest Young's modulus is along the *c* axis for the sc-form but tilting an angle from the *c* axis for the β-form. The *ca* plane is $\varphi_0 = 0°$, and the *cb* plane $\varphi_0 = 120°$.

3.3. Elastic Properties for Polycrystalline Aggregates. The stiffness tensor completely specifies the elastic properties and acoustic velocities of a single crystal. It is interesting to compute the elastic properties of a polycrystalline aggregate. Once the elastic stiffness and compliance of a single crystal are determined, one can estimate the elastic properties of polycrystals by averaging over different orientations of the single crystal if ignoring the gain boundaries and defects. The lower and upper bounds of the isotropic bulk modulus *K*, shear modulus *G* are given by Reuss[32] and Voigt,[33] respectively. The effect moduli could be approximated by the arithmetic mean of the two bounds.[34] However, for polymers, the actual results could be close to one of the bounds.

It is more complicated to estimate the bulk properties of polymer samples because of the existence of amorphous regions and interconnections between the crystalline and amorphous regions. The bulk properties depend on many factors such as the degree of crystallinity, orientation, etc. Normally, composite models are used. Nevertheless, we can use the values of the simplified polycrystalline aggregate models to represent the upper bounds on the isotropic moduli based on the calculated lower Reuss and upper Voigt bounds.

3.3.1. Unoriented-Random Isotropic Aggregates. Assuming the stiffness and compliance constants of a single crystal are c_{pq} and s_{pq}, the isotropic averaged $\bar{c}'_{pq}$ and $\bar{s}'_{pq}$ are given by

(1) For single crystal units having orthorhombic symmetry[35]

Voigt (uniform strain): the isotropic averaged stiffness components $\bar{c}'_{pq}$ were given in eqs 30−32 in ref 35.

Reuss (uniform stress): the isotropic averaged compliance components $\bar{s}'_{pq}$ were given in eqs 33−35 in ref 35.

(2) For single crystal units possessing transversely isotropic symmetry[36]

$$c_{11} = c_{22}, c_{13} = c_{23}, c_{44} = c_{55}, c_{66} = \frac{1}{2}(c_{11} - c_{12})$$

$$s_{11} = s_{22}, s_{13} = s_{23}, s_{44} = s_{55}, s_{66} = 2(s_{11} - s_{12})$$

Voigt (uniform strain): the isotropic averaged stiffness components $\bar{c}'_{pq}$ were given in eqs 5.14 and 5.16 in ref 36.

Reuss (uniform stress): the isotropic averaged compliance components $\bar{s}'_{pq}$ were given in eqs 5.13 and 5.15 in ref 36.

For an isotropic material, the stiffness matrix can be fully described by only two independent coefficients: the so-called the Lame coefficients λ and μ,

$$\begin{bmatrix} \lambda + 2\mu & \lambda & \lambda & 0 & 0 & 0 \\ \lambda & \lambda + 2\mu & \lambda & 0 & 0 & 0 \\ \lambda & \lambda & \lambda + 2\mu & 0 & 0 & 0 \\ 0 & 0 & 0 & \mu & 0 & 0 \\ 0 & 0 & 0 & 0 & \mu & 0 \\ 0 & 0 & 0 & 0 & 0 & \mu \end{bmatrix}$$

where $\mu = \bar{c}'_{44}$, $\lambda = \bar{c}'_{12}$, and $\lambda + 2\mu = \bar{c}'_{11}$. Then elastic properties for the isotropic case can be written in terms of the Lame coefficients: Young's modulus $E = \mu[(3\lambda + 2\mu)/(\lambda + \mu)]$, Poisson's ratio $\nu = \lambda/2(\mu + \lambda)$, bulk modulus $K = \lambda + {}^2/_3\mu$, and shear modulus $G = \mu$.

The calculated bulk modulus *K*, shear modulus *G*, Young's modulus *E*, and Poisson's ratio for the three PLA crystals are given in Table 2. The isotropic aggregate of α-PLLA has the highest effect Young's and shear moduli. It is worthy noting, however, that in real polymer systems, the sc-PLLA-PDLA system may lead to fast crystallization and high crystallinity,

which results in a higher Young's modulus compared with that from the pure α-PLLA polymer system.

3.3.2. uniaxially Oriented-Cylindrically Symmetric Aggregates. Drawn fibers show isotropy in a plane perpendicular to the direction of drawing; the number of independent elastic constants is 5. Choose the z direction along the polymer chain helix axis in single crystals and z' the fiber drawing direction.

(1) A transversely isotropic aggregate of orthorhombic units[35,37]

In the general transformation eqs 18−29 of ref 35, if $\theta = 0$ and we average over angle Ω, $(1/2\pi)\int_0^{2\pi} f(\Omega)\, d\Omega$, one gets the Reuss average fiber compliance components as

$$\bar{s}'_{33} = s_{33}, \bar{s}'_{11} = \frac{3}{8}s_{11} + \frac{1}{4}s_{12} + \frac{3}{8}s_{22} + \frac{1}{8}s_{66},$$
$$\bar{s}'_{12} = \frac{1}{8}s_{11} + \frac{3}{4}s_{12} + \frac{1}{8}s_{22} - \frac{1}{8}s_{66}$$

$$\bar{s}'_{13} = \frac{1}{2}(s_{13} + s_{23}), \bar{s}'_{44} = \frac{1}{2}(s_{44} + s_{55}), \bar{s}'_{66} = 2(\bar{s}'_{11} - \bar{s}'_{12})$$

and the Voigt average fiber constants, in a similar way, are

$$\bar{c}'_{33} = c_{33}, \bar{c}'_{11} = \frac{3}{8}c_{11} + \frac{1}{4}c_{12} + \frac{3}{8}c_{22} + \frac{1}{2}c_{66},$$
$$\bar{c}'_{12} = \frac{1}{8}c_{11} + \frac{3}{4}c_{12} + \frac{1}{8}c_{22} - \frac{1}{2}c_{66}$$

$$\bar{c}'_{13} = \frac{1}{2}(c_{13} + c_{23}), \bar{c}'_{44} = \frac{1}{2}(c_{44} + c_{55}), \bar{c}'_{66} = \frac{1}{2}(\bar{c}'_{11} - \bar{c}'_{12})$$

(2) A transversely isotropic aggregate of transverse isotropic symmetry units[37]

$$c_{11} = c_{22}, c_{13} = c_{23}, c_{44} = c_{55}, c_{66} = \frac{1}{2}(c_{11} - c_{12})$$

$$s_{11} = s_{22}, s_{13} = s_{23}, s_{44} = s_{55}, s_{66} = 2(s_{11} - s_{12})$$

Voigt:

$$\bar{c}'_{33} = c_{33}, \bar{c}'_{11} = \frac{3}{8}c_{11} + \frac{1}{4}c_{12} + \frac{3}{8}c_{22} + \frac{1}{2}c_{66} = c_{11},$$
$$\bar{c}'_{12} = \frac{1}{8}c_{11} + \frac{3}{4}c_{12} + \frac{1}{8}c_{22} - \frac{1}{2}c_{66} = c_{12}$$

$$\bar{c}'_{13} = \frac{1}{2}(c_{13} + c_{23}) = c_{13}, \bar{c}'_{44} = \frac{1}{2}(c_{44} + c_{55}) = c_{44},$$
$$\bar{c}'_{66} = \frac{1}{2}(\bar{c}'_{11} - \bar{c}'_{12}) = c_{66}$$

Reuss:

$$\bar{s}'_{33} = s_{33}, \bar{s}'_{11} = \frac{3}{8}s_{11} + \frac{1}{4}s_{12} + \frac{3}{8}s_{22} + \frac{1}{8}s_{66} = s_{11},$$
$$\bar{s}'_{12} = \frac{1}{8}s_{11} + \frac{3}{4}s_{12} + \frac{1}{8}s_{22} - \frac{1}{8}s_{66} = s_{12}$$

$$\bar{s}'_{13} = \frac{1}{2}(s_{13} + s_{23}) = s_{13}, \bar{s}'_{44} = \frac{1}{2}(s_{44} + s_{55}) = s_{44},$$
$$\bar{s}'_{66} = 2(\bar{s}'_{11} - \bar{s}'_{12}) = s_{66}$$

Extensional (Young's) modulus and Poisson's ratio: $E_3 = 1/\bar{s}'_{33}$, $\nu_{13} = -\bar{s}'_{13}/\bar{s}'_{33}$

Transverse Modulus and Poisson's ratio: $E_1 = 1/\bar{s}'_{11}$, $\nu_{12} = -\bar{s}'_{12}/\bar{s}'_{11}$, $\nu_{31} = -\bar{s}'_{31}/\bar{s}'_{11}$

Torsional (shear) Modulus: $G = 1/\bar{s}'_{44} = 1/\bar{s}'_{55}$, these relate to torsion about the symmetry axis z, i.e., shear in the yx or zx planes.

TABLE 2: Calculated Bulk Moduli, K_V, K_R, and $K_H = (K_R + K_V)/2$, Shear Moduli G_V, G_R, and $G_H = (G_R + G_V)/2$, Young's Modulus E and Posson's Ratio ν, for Isotropic Polycrystalline Poly(lactic acid) Aggregates[a]

individual units	bounds	K	G	E	ν
α-PLLA	Voigt	11.41 (11.21)	6.70 (4.97)	16.81 (12.98)	0.25 (0.31)
	Reuss	6.61 (8.69)	4.07 (3.54)	10.14 (9.36)	0.24 (0.32)
	Hill	9.01 (9.95)	5.39 (4.25)	13.47 (11.17)	0.25 (0.31)
β-PLLA	Voigt	18.37	5.05	13.88	0.37
	Reuss	13.13	1.96	5.60	0.43
	Hill	15.75	3.50	9.74	0.40
sc- PLLA:PDLA =50:50	Voigt	12.61	3.37	9.28	0.38
	Reuss	11.62	1.64	4.69	0.43
	Hill	12.11	2.50	6.99	0.41

[a] Values in brackets are obtained from stiffness and compliance calculated using a forcefield method for PLLA α-phase.[14] All the moduli are in GPa.

TABLE 3: Calculated Elastic Properties of a Cylindrically Symmetric Aggregate of PLA Crystals[a]

crystal	bounds	E_1 (GPa)	E_3 (GPa)	G (GPa)	ν_{12}	ν_{13}	ν_{31}
α-PLLA	Voigt	7.92 (9.18)	16.36 (36.05)	10.58 (3.05)	0.17 (0.44)	0.61 (0.33)	0.29 (0.085)
	Reuss	6.30 (8.99)	14.13 (35.97)	10.03 (3.00)	0.11 (0.44)	0.71 (0.34)	0.32 (0.085)
β-PLLA	Voigt	4.78	7.14	9.46	0.31	0.63	0.42
	Reuss	3.50	7.14	6.08	0.50	0.63	0.31
sc-PLLA: PDLA = 50:50	Voigt	11.88	15.26	0.82	0.18	0.46	0.35
	Reuss	11.85	15.26	0.82	0.18	0.45	0.35

[a] Values in brackets are calculated from stiffness calculated using a force field method for the α-phase.[14]

Table 3 lists the calculated elastic properties of oriented fibers. Interestingly, the sc-form has very strong moduli in both the fiber and the transverse directions and a very small shear modulus. Uniaxially oriented stererocomplex crystal aggreage can enhances the fiber Young's moduli in the fiber direction as well as in the transverse direction and reduces the shear modulus.

4. Conclusions

We have calculated stiffness and compliance of the three possible crystal structures of poly(lactic acid) by employing a DFT stress−strain method. Stiffness coefficient along the polymer helix axis direction (c_{33}) is greater than those in the transverse directions (c_{11} and c_{22}). Young's modulus and linear compressibility of the single crystals are anisotropic. However, both the β-form and sc-form show transversely isotropic. In addition, the sc-form has a higher Young's modulus and less compressibility than the β-form in the *ab* plane. The Voigt and Reuss bounds for the isotropic and uniaxially oriented fiber were estimated on the basis of simplified polycrystalline aggregate models. For real semicrystalline PLA samples, the amorphous regions should be considered as well. The α-PLLA isotropic aggregate has the highest Young's and shear moduli. Uniaxially orienting stereocomplex crystals can increase the fiber Young's modulus and reduce shear modulus.

References and Notes

(1) Tsuji, H. *Macromol. Biosci.* **2005**, *5*, 569.
(2) Anderson, K. S.; Schreck, K. M.; Hillmyer, M. A. *Polym. Rev.* **2008**, *48*, 85.
(3) Fukuda, E. *Rep. Prog. Polym. Phys. Jpn.* **1991**, *34*, 269.
(4) Ochiai, T.; Fukada, E. *Jpn. J. Appl. Phys.* **1998**, *37*, 3374.
(5) Tajitsu, Y.; Kanesaki, M.; Tsukiji, M.; Imoto, K.; Date, M.; Fukada, E. *Ferroelectrics* **2005**, *320*, 601.
(6) De Santis, P.; Kovacs, A. *Biopolymers* **1968**, *6*, 299.
(7) Eling, B.; Gogolewski, S.; Pennings, A. J. *Polymer* **1982**, *23* (11), 1587.
(8) Ikada, Y.; Jamshidi, K.; Tsuji, H.; Hyon, S. H. *Macromolecules* **1987**, *20* (4), 904.
(9) Cartier, L.; Okihara, T.; Ikada, Y.; Tsuji, H.; Puiggali, J.; Lotz, B. *Polymer* **2000**, *41* (25), 8909.
(10) Kobayashi, J.; Asahi, T.; Ichiki, M.; Oikawa, A.; Suzuki, H.; Watanabe, T.; Fukada, E.; Shikinami, Y. *J. Appl. Phys.* **1995**, *77* (7), 2957.
(11) Aleman, C.; Lotz, B.; Puiggali, J. *Macromolecules* **2001**, *34* (14), 4795.
(12) Sasaki, S.; Asakura, T. *Macromolecules* **2003**, *36* (22), 8385.
(13) Puiggali, J.; Ikada, Y.; Tsuji, H.; Cartier, L.; Okihara, T.; Lotz, B. *Polymer* **2000**, *41* (25), 8921.
(14) De Oca, H. M.; Ward, I. M. *J. Polym. Sci. Part B-Polym. Phys.* **2007**, *45* (8), 892.
(15) Nielsen, O. H.; Martin, R. M. *Phys. Rev. B* **1985**, *32*, 3780.
(16) Nielsen, O. H.; Martin, R. M. *Phys. Rev. B* **1985**, *32*, 3792.
(17) Milman, V.; Winkler, B.; White, J. A.; Pickard, C. J.; Payne, M. C.; Akhmatskaya, E. V.; Nobes, R. H. *Int. J. Quantum Chem.* **2000**, *77*, 895.
(18) Clark, S. J.; Segall, M. D.; Pickard, C. J.; Hasnip, P. J.; Probert, M. I. J.; Refson, K.; Payne, M. C. *Z. Kristallogr.* **2005**, *220*, 567.
(19) Segall, M. D.; Lindan, P. J. D.; Probert, M. J.; Pickard, C. J.; Hasnip, P. J.; Clark, S. J.; Payne, M. C. *J. Phys.-Condens. Matter* **2002**, *14* (11), 2717.
(20) Hohenber, P.; Kohn, W. *Phys. Rev.* **1964**, *136*, 864.
(21) Kohn, W.; Sham, L. J. *Phys. Rev. A* **1965**, *140*, 113.
(22) Nielsen, O. H.; Martin, R. M. *Phys, Rev. Lett.* **1983**, *50*, 697.
(23) Mehl, M. J.; Osburn, J. E.; Papaconstantopoulos, D. A.; Klein, B. M. *Phys. Rev. B* **1990**, *41*, 10311.
(24) Fischer, E. W.; Sterzel, H. J.; Wegner, G. *Kolloid-Z. u. Z. Polymere* **1973**, *251*, 980.
(25) Meijer, E. J.; Sprik, M. *J. Chem. Phys.* **1996**, *105* (19), 8684.
(26) Steinle-Neumann, G.; Strixrude, L.; Cohen, R. E. *Phys. Rev. B* **1999**, *60*, 791–799.
(27) Vanderbilt, D. *Phys. Rev. B* **1990**, *41*, 7892.
(28) Payne, M. C.; Teter, M. P.; Allan, D. C.; Arias, T. A.; Joannopoulos, J. D. *Rev. Mod. Phys.* **1992**, *64* (4), 1045.
(29) Perdew, J. P.; Wang, Y. *Phys. Rev. B* **1992**, *45* (23), 13244.
(30) Monkhorst, H. J.; Pack, J. D. *Phys. Rev. B* **1976**, *13*, 5188.
(31) Nye, J. F. *Physical Properties of Crystals*; Clarendon: Oxford, U.K., 1957.
(32) Reuss, A. Z. *Angew. Math. Mech.* **1929**, *8*, 55.
(33) Voigt, W. *Lehrbush der Kristallphysik*; Taubner: Leipzig, 1928.
(34) Hill, R. *Proc. Phys. Soc. London A* **1952**, *65*, 349.
(35) Read, B. E.; Dean, G. *Polymer* **1970**, *11*, 597.
(36) Ward, I. M. *Proc. Phys. Soc.* **1962**, *80*, 1176.
(37) Ward, I. M. *Mechanical Properties of Solid Polymers*, 2nd ed.; John Wiley & Sons: New York, 1983; pp 296−297.

JP911198P